Torque and Velocity Ripple Elimination of AC Permanent Magnet Motor Control Systems Using the Internal Model Principle

Wai-Chuen Gan, *Member, IEEE* and Li Qiu, *Senior Member, IEEE*

***Abstract*—This paper addresses the problem of torque and velocity ripple elimination in AC permanent magnet (PM) motor control systems. The torque ripples caused by DC offsets that are present in the current sensors of the motor driver and the digital-to-analog converters of the motion controller are studied and formulated mathematically. These torque ripples eventually generate velocity ripples at the speed output and degrade the system performance. In this paper the torque ripples are modeled as a sinusoidal function with a frequency depending on the motor speed. The internal model principle (IMP) is then used to design a controller to eliminate the torque and velocity ripples without estimating the amplitude and the phase values of the sinusoidal disturbance. A gain scheduled (GS) robust two degree of freedom (2DOF) speed regulator based on the IMP and the pole-zero placement is developed to eliminate the torque and velocity ripples and achieve a desirable tracking response. Simulation and experimental results reveal that the proposed GS robust 2DOF speed regulator can effectively eliminate the torque ripples generated by DC current offsets, and produce a velocity ripple-free output response.**

***Index Terms*—AC permanent magnet motor, gain scheduled (GS) speed regulators, internal model principle (IMP), sinusoidal disturbance, torque and velocity ripple elimination.**

I. Introduction

PRECISION speed-control systems are crucial in numerous industrial applications. For example, one typical application can be found in the feed control of machine tools in the manufacturing industry where accurate smooth position and speed control are required for contour accuracy and small surface roughness of the products [1], [2].

AC permanent magnet (PM) motors are attractive candidates for high-performance industrial control applications such as the one stated above. The maintenance of AC PM motors is minimal because of the brushless rotor construction. In addition, AC PM motors have higher power to volume ratios than DC motors have. However, the torque ripple generation in AC PM motor systems limits the applications of AC PM motors in high-performance speed and position control systems. In general, the disturbance torque ripples of AC PM motor control systems are composed of cogging torque, reluctance torque, mutual torque and the DC current offset torque that is caused by the DC offsets of the current sensors in the motor driver and the digital-to-analog converters in the motion controller [3], [4]. The cogging and reluctance torque ripples are usually very small in magnitude for optimally designed AC PM motors [9]; the mutual torque ripples are present at the high frequency range (multiples of six electrical shaft speed) and are often attenuated substantially by the output mechanical systems [3]; the torque ripples due to current offsets are dominant among the above four types of ripples in a typical AC PM motor control system as the offsets from the current sensors and digital-to-analog converters are difficult to eliminate. In addition, the output mechanical system responses can be deteriorated because of the low-fundamental frequency of DC current offset torque ripples in comparison to that of mutual torque ripples. There are many different techniques to eliminate the torque ripples of AC PM motor control systems [5]. These techniques can be divided into two categories. In the first category, machine design is optimized so as to eliminate the cogging and reluctance torque ripple generation of AC PM motors [6], [7]. In the second category, different adaptive control algorithms have been applied to eliminate the torque ripple of AC PM motor control systems [3], [4], [8]. In these adaptive control algorithms, the amplitude and the phase values of the torque ripple disturbance are first estimated and then used in the motor controller to cancel the torque ripples.

In a practical high-performance AC PM motor control system, the basic components consist of a motion controller, a current tracking amplifier, a feedback encoder and an AC PM motor as shown in Fig. 1. DC offsets are always present at the motor terminals due to the digital-to-analog converter offsets of the motion controller and the current sensor offsets of the current tracking amplifier. These current offsets generate sinusoidal torque disturbances and, hence, produce velocity ripples at the system output. The present literature [3], [6]–[8] concerns mostly the elimination of the cogging torque, reluctance torque, and mutual torque, and there is not much research devoted to the elimination of the torque ripples caused by DC current offsets. In the past, the way to eliminate these torque ripples was to purchase high grade and expensive current sensors and digital-to-analog converters to minimize the DC offset values, respectively; skillful operators or service engineers were required to trim the offset values periodically as these DC offset values drift with time slowly. The total cost of an automation machine is thus much increased. To replace the above inefficient and high-cost solutions, the development of a novel and cost-effective speed control algorithm to eliminate the torque rip-

Manuscript received January 28, 2002; revised January 20, 2003. This work was supported by the Hong Kong Research Grants Council under Grants HKUST6046/00E and HKUST6032/01E.

W.-C. Gan was with the Department of Electrical and Electronic Engineering, The Hong Kong University of Science and Technology, Hong Kong. He is now with ASM Assembly Automation Ltd., Hong Kong, Hong Kong.

L. Qiu is with the Department of Electrical and Electronic Engineering, The Hong Kong University of Science and Technology, Hong Kong, Hong Kong (e-mail: eeqiu@ee.ust.hk).

Digital Object Identifier 10.1109/TMECH.2004.828626

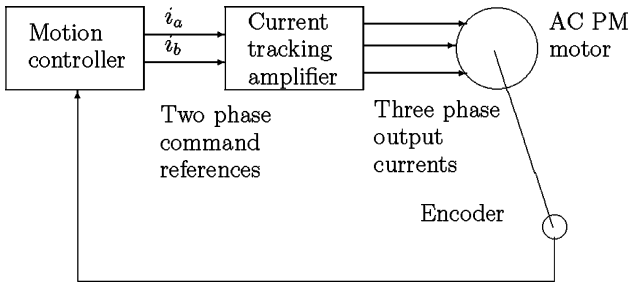

Fig. 1. AC PM motor control system.

ples caused by DC current offsets is discussed in this paper. This proposed control algorithm can be classified into the second category as mentioned before but without estimating the amplitude and the phase values of the disturbance explicitly.

In this paper, the AC PM motor used in the motor control system is assumed to be well designed so that the cogging torque, reluctance torque, and mutual torque can be neglected, and this assumption is often valid in high-performance applications [3], [9]. On the other hand, we focus on the elimination of the torque ripples caused by DC current offsets. The torque ripples caused by DC current offsets can be modeled by a sinusoidal function with a known frequency. The disturbance frequency has a fixed relationship with the speed input reference. The internal model principle (IMP) is applied in the motor controller design to eliminate the torque ripples without estimating the amplitude and the phase values of the sinusoidal disturbance. A gain scheduled (GS) robust two degrees of freedom (2DOF) speed regulator based on the IMP and the pole-zero placement algorithm is designed so as to achieve a desirable and velocity ripple-free output response for a time-varying step reference input.

This paper is organized as follows. In Section II, a brief review on the vector control of AC PM motors and the modeling of the torque ripples caused by DC current offsets is given. In Section III, the use of the IMP is proposed to eliminate the sinusoidal disturbance without estimating its amplitude and phase values. As the disturbance frequency has a fixed relationship with the input reference, the internal modes change with the command input; thus, a GS robust 2DOF speed regulator based on the IMP and the pole-zero placement algorithm is developed for a time-varying step reference input. The stability issue of the proposed GS robust 2DOF speed regulator is addressed. An improved GS robust 2DOF speed regulator with the acceleration profile input is then developed to enlarge the system stability radius. The simulation results of the proposed GS robust 2DOF speed regulators are presented in Section IV. In Section V, experimental results are compared with the simulation results to validate our control methodology. Some concluding remarks are given in Section VI.

II. Vector Control of AC PM Motors and Disturbance Modeling

In this section, the vector control of AC PM motors is reviewed and the modeling of the torque ripple disturbance caused by the DC current offsets is discussed. A three phase AC PM motor can be modeled in the $d-q$ frame by the following [10]:

$$v_d(t) = R_s i_d(t) + \frac{L_d di_d(t)}{dt} - \omega_e(t) L_q i_q(t) \quad (1)$$

$$v_q(t) = R_s i_q(t) + \frac{L_q di_q(t)}{dt} + \omega_e(t)\left(L_d i_d(t) + \lambda_m\right) \quad (2)$$

$$\tau_e(t) = \frac{3}{2}\frac{P}{2}\left[\lambda_m i_q(t) - (L_q - L_d) i_d(t) i_q(t)\right] \quad (3)$$

and

$$\tau_e(t) - \tau_l(t) = J_m \frac{d\omega(t)}{dt} + B_m \omega(t) \quad (4)$$

where the parameters and variables have the following meanings:

R_s	stator winding resistance;
P	number of poles (even number);
L_d, L_q	$d-q$ frame stator synchronous inductances;
J_m	moment of inertia;
B_m	friction constant;
λ_m	constant magnetic flux;
$v_d(t)$, $v_q(t)$	$d-q$ frame stator voltages;
$i_d(t)$, $i_q(t)$	$d-q$ frame stator currents;
$\tau_e(t)$	electro-mechanical torque;
$\tau_l(t)$	load torque;
$\omega(t)$	rotor mechanical speed;
$\omega_e(t) = (P/2)\omega(t)$	rotor electrical speed.

The electrical time constants L_d/R_s and L_q/R_s are usually much smaller than the dominant time constant of the outer speed loop. For example, the bandwidth of the current loop is always in the order of kilo hertz and the bandwidth of the outer speed loop is in the order of 10 Hz generally. With a well-tuned current loop controller, the dynamic equations (1) and (2) can be eliminated. In this case, $i_d(t)$ and $i_q(t)$ become the system inputs. Furthermore, the vector control technique suggests to set $i_d(t) = 0$. This converts the nonlinear AC PM motor system into a linear system

$$\tau_e(t) = \frac{3}{2}\frac{P}{2}\lambda_m i_q(t)$$

$$\tau_e(t) - \tau_l(t) = J_m \frac{d\omega(t)}{dt} + B_m \omega(t).$$

When the motor current amplifier is connected to the power source and the two current reference commands from the motion controller are kept at zero, a DC offset current induced by the current sensor offsets and the digital-to-analog converter offsets may be present in one or both of the closed loop controlled phases and, thus, also in the third one [4]. Let I_a, I_b be the two DC current offsets present at the motor terminals due to the digital-to-analog converter offsets of the motion controller and the current sensor offsets of the current amplifier. Then $I_c = -(I_a + I_b)$ is the third phase current offset, as shown in (5) at the bottom of the next page.

Let $i_a^*(t)$, $i_b^*(t)$ and $i_c^*(t)$ be the desired currents at the motor terminals. When the three phase currents with offsets enter the motor, the actual currents, $i_q(t)$, $i_d(t)$ and $i_0(t)$ can be computed using the forward (abc frame to $dq0$ frame) transformation as in (5), [10], [13], where $\theta_e(t) + (\pi/2)$ is the commutation angle

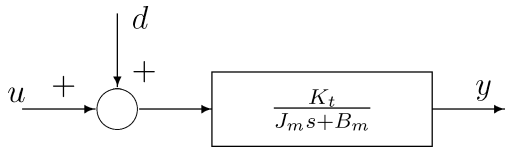

Fig. 2. System model with disturbance.

for an AC PM motor and $\theta_e(t) = \theta_e(0) + \int_0^t \omega_e(t)dt$ is the electrical angle. Then $i_q(t)$ is given by

$$i_q(t) = i_q^*(t) + i_{\text{qoff}}(t)$$

where

$$i_q^*(t) = \frac{2}{3}\left[i_a^*(t)\cos\left(\theta_e(t)+\frac{\pi}{2}\right) + i_b^*(t)\cos\left(\theta_e(t)-\frac{\pi}{6}\right) + i_c^*(t)\cos\left(\theta_e(t)+\frac{7\pi}{6}\right)\right]$$

is the desired current value at q axis. The disturbance term

$$i_{\text{qoff}}(t) = \frac{2}{3}\left\{I_a\left[\cos\left(\theta_e(t)+\frac{\pi}{2}\right) - \cos\left(\theta_e(t)+\frac{7\pi}{6}\right)\right] + I_b\left[\cos\left(\theta_e(t)-\frac{\pi}{6}\right) - \cos\left(\theta_e(t)+\frac{7\pi}{6}\right)\right]\right\}. \quad (6)$$

Similarly, for the d axis current

$$i_d(t) = i_d^*(t) + i_{\text{doff}}(t)$$

where $i_d^*(t)$ is the desired current value at d axis and is equal to 0 by employing vector control. The remaining disturbance term is

$$i_{\text{doff}}(t) = \frac{2}{3}\left\{I_a\left[\sin\left(\theta_e(t)+\frac{\pi}{2}\right) - \sin\left(\theta_e(t)+\frac{7\pi}{6}\right)\right] + I_b\left[\sin\left(\theta_e(t)-\frac{\pi}{6}\right) - \sin\left(\theta_e(t)+\frac{7\pi}{6}\right)\right]\right\}.$$

Finally $i_0(t)$ in (5) is still equal to zero since $i_a^*(t) + i_b^*(t) + i_c^*(t) = 0$. For surface PM rotor type AC servo motors, which are popular in various industrial applications, we have $L_d = L_q$ [14]. With this property, the torque generation (3) can be simplified as

$$\tau_e(t) = \tau_e^*(t) + \tau_{\text{off}}(t)$$

where

$$\tau_e^*(t) = \frac{3}{2}\frac{P}{2}\lambda_m i_q^*(t)$$

is the desired torque and

$$\tau_{\text{off}}(t) = \frac{3}{2}\frac{P}{2}\lambda_m i_{\text{qoff}}(t) \quad (7)$$

is the offset torque. Substituting (6) into (7), we get

$$\tau_{\text{off}}(t) = \frac{P}{2}\lambda_m I_a\left[-\frac{3}{2}\sin(\theta_e(t)) + \frac{\sqrt{3}}{2}\cos(\theta_e(t))\right] + \frac{P}{2}\lambda_m I_b\left[\sqrt{3}\cos(\theta_e(t))\right].$$

Physically, the interaction of the rotating magnetic field excited by the permanent magnet and the stationary magnetic field excited by the DC current flowing in the stator windings will generate sinusoidal torque ripples. Mathematically, when the output mechanical speed tracks closely with the reference input at the steady state, it follows that the relationship $\omega_d(t) = \omega_e(t) \approx (P/2)\omega_r(t)$ can be assumed where $\omega_d(t)$ is defined as the disturbance torque can then be further simplified and approximated by a sinusoidal function

$$\tau_{\text{off}}(t) = A_d\cos(\omega_d(t)t - \phi_d) \quad (8)$$

where A_d is the magnitude of the disturbance while ϕ_d is the phase of the disturbance. The disturbance frequency, $\omega_d(t)$, is a slowly time-varying function in comparison to the cosine function.

In summary, after employing the vector control and the formulation of the sinusoidal disturbance, the model of a vector controlled AC PM motor with the torque ripple disturbance is given by Fig. 2. Here, $u(t) = i_q^*(t)$ is the input current, $y(t) = \omega(t)$ is the output mechanical speed, $K_t = (3/2)(P/2)\lambda_m$ is the equivalent torque constant, $d(t) = (\tau_{\text{off}}(t) + \tau_l(t))/(K_t)$ where $\tau_l(t)$ is the load torque which can be considered as an unknown constant disturbance, $\tau_{\text{off}}(t)$ is the torque disturbance due to DC current offsets, and can be approximated by a sinusoidal function with a known frequency $\omega_d(t)$ and an unknown magnitude and phase. Our goal is to design a speed controller so that the output speed tracks a constant reference or a time-varying step reference and rejects the disturbance $\tau_{\text{off}}(t)$ and $\tau_l(t)$. Such a controller is required to be robust, i.e. to perform the tracking and disturbance rejection even when the system parameters vary slightly, to have a good transient response, and to have low complexity, i.e., to have an order as low as possible.

To eliminate completely and robustly the sinusoidal disturbance with the known frequency, the use of the IMP is necessary. The IMP calls the use of the modes of the disturbance in the controller as internal modes of the feedback loop. The estimation of the amplitude and the phase values of the disturbance is not necessary in the elimination of the sinusoidal disturbance. In the next section, the development of speed regulators with the internal modes of the disturbance for an AC PM motor control system is addressed. The speed regulator is first designed with the consideration of a constant speed reference so that the internal modes inside the speed controller are fixed too. Then a GS speed regulator is designed for a time-varying step reference.

$$\begin{bmatrix} i_q(t) \\ i_d(t) \\ i_0(t) \end{bmatrix} = \frac{2}{3}\begin{bmatrix} \cos\left(\theta_e(t)+\frac{\pi}{2}\right) & \cos\left(\theta_e(t)-\frac{\pi}{6}\right) & \cos\left(\theta_e(t)+\frac{7\pi}{6}\right) \\ \sin\left(\theta_e(t)+\frac{\pi}{2}\right) & \sin\left(\theta_e(t)-\frac{\pi}{6}\right) & \sin\left(\theta_e(t)+\frac{7\pi}{6}\right) \\ \frac{1}{2} & \frac{1}{2} & \frac{1}{2} \end{bmatrix}\begin{bmatrix} i_a^*(t)+I_a \\ i_b^*(t)+I_b \\ i_c^*(t)+I_c \end{bmatrix} \quad (5)$$

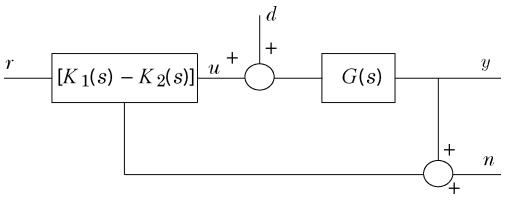

Fig. 3. A 2DOF controller structure.

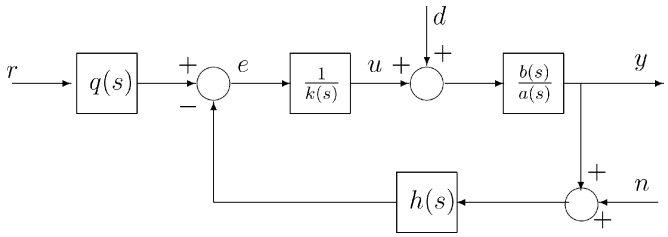

Fig. 4. The 2DOF regulator structure.

III. Controller Design

The problem of accomplishing robust tracking and disturbance rejection is called the robust regulator problem. The key idea to solve a robust regulator problem is, based on the IMP, to have the controller to include the modes of the reference and disturbance. We also propose to use a 2DOF controller structure to achieve better transient responses and simpler designs. A 2DOF controller has a structure as shown in Fig. 3 with n denotes the sensor noise. One of its advantages, in comparison with the usual one degree of freedom or unity feedback structure, which amounts to setting $K_1(s) = K_2(s)$, is that the tracking performance depends mainly on $K_1(s)$, and the robustness and the disturbance rejection performance depends only on $K_2(s)$. Hence $K_1(s)$ and $K_2(s)$ can be designed with different considerations.

In this section, we first carry out the design of a linear time invariant (LTI) robust 2DOF controller for a constant speed reference. Then a GS robust 2DOF controller for a slowly time-varying speed step reference is designed by modifying the LTI controller.

A. Controller Design for a Constant Reference

In this section, the input reference is assumed to be a constant value ω_r so that $\omega_d = (P/2)\omega_r$. The 2DOF regulator structure employed in our analysis is shown in Fig. 4. Here we follow the design procedure for the robust 2DOF regulator using pole-zero placement technique given in Appendix A. For our PM motor control system, in reference to Fig. 4, we have $a(s) = s + (B_m/J_m)$ and $b(s) = (K_t/J_m)$. Since the reference $r(t)$ is a step reference, it follows that $m_r(s) = s$. Since the disturbance $d(t)$ contains a sinusoidal function of frequency $\omega_d = (P/2)\omega_r$ and a constant function, it follows that $m_d(s) = s(s^2 + \omega_d^2)$. Therefore, $m(s) = s(s^2 + \omega_d^2)$. It follows that $m(s)a(s)$ and $b(s)$ are coprime and a solution to the robust regulator problem based on the IMP exists. Since $n_a = 1$, we can choose $n_g = 0$ according to (33). This leads to a controller of order equal to n_m, which is the lowest possible to achieve robust regulator. Hence

$$k(s) = m(s) = s\left(s^2 + \omega_d^2\right) \tag{9}$$

and $h(s)$ and $q(s)$ have the following forms:

$$\begin{aligned} h(s) &= h_0 s^3 + h_1 s^2 + h_2 s + h_3 \\ q(s) &= q_0 s^3 + q_1 s^2 + q_2 s + q_3. \end{aligned}$$

Choose the closed loop poles α_1, α_2 and α_3 according to the disturbance rejection specification and the remaining closed loop pole α_4 according to the transient tracking response specification so that the closed loop characteristic polynomial is

$$\begin{aligned} \delta(s) &= (s+\alpha_1)(s+\alpha_2)(s+\alpha_3)(s+\alpha_4) \\ &= s^4 + \delta_1 s^3 + \delta_2 s^2 + \delta_3 s + \delta_4. \end{aligned}$$

Then by equating the coefficients of both sides of

$$\delta(s) = k(s)a(s) + b(s)h(s)$$

we can obtain

$$h_0 = \frac{J_m}{K_t}\left(\delta_1 - \frac{B_m}{J_m}\right) \tag{10}$$

$$h_1 = \frac{J_m}{K_t}\left(\delta_2 - \omega_d^2\right) \tag{11}$$

$$h_2 = \frac{J_m}{K_t}\left(\delta_3 - \omega_d^2\frac{B_m}{J_m}\right) \tag{12}$$

$$h_3 = \frac{J_m}{K_t}\delta_4. \tag{13}$$

Finally, as $m_r(s) = s$, we can arbitrarily assign the roots of $q(s)$. Here we choose the three roots of $q(s)$ to be exactly the same as three roots of $\delta(s)$ subject to the constraint $q_3 = h_3$

$$q(s) = \frac{h_3}{\alpha_1\alpha_2\alpha_3}(s+\alpha_1)(s+\alpha_2)(s+\alpha_3) \tag{14}$$

where

$$\begin{aligned} q_0 &= \frac{h_3}{\alpha_1\alpha_2\alpha_3} \\ q_1 &= \frac{h_3(\alpha_1+\alpha_2+\alpha_3)}{\alpha_1\alpha_2\alpha_3} \\ q_2 &= \frac{h_3(\alpha_1\alpha_2+\alpha_2\alpha_3+\alpha_3\alpha_1)}{\alpha_1\alpha_2\alpha_3} \\ q_3 &= h_3. \end{aligned}$$

In this way, the system from r to y is turned to a first order system with a pole determined by the remaining root of $\delta(s)$ and the transfer function is given by

$$\frac{Y(s)}{R(s)} = \frac{\alpha_4}{s+\alpha_4}.$$

B. Controller Design for a Slowly Time-Varying Step Reference

The robust 2DOF regulator described in the previous section is designed for a constant speed reference so that the tracking error is zero at the steady state. However, there are many industrial applications that require a varying speed operation. In this case, the sinusoidal disturbance has a varying frequency. In order to achieve zero steady state error, we need to include an internal mode which varies with the disturbance frequency; other parameters of the controller in general also need to be changed with time to ensure that the closed loop system, which is time-varying, is internally and externally stable. In this section the development of a GS robust 2DOF regulator for a time-varying

step reference to eliminate the torque and velocity ripples of AC PM motors, is discussed.

The idea behind the GS robust 2DOF pole-zero placement regulator is to replace the disturbance frequency ω_d in (9) and (10)–(13) by $\omega_d(t) = (P/2)\omega_r(t)$ as follows:

$$k_2(t) = \omega_d^2(t) \tag{15}$$

$$h_0(t) = \frac{J_m}{K_t}\left(\delta_1 - \frac{B_m}{J_m}\right) \tag{16}$$

$$h_1(t) = \frac{J_m}{K_t}\left(\delta_2 - \omega_d^2(t)\right) \tag{17}$$

$$h_2(t) = \frac{J_m}{K_t}\left(\delta_3 - \omega_d^2(t)\frac{B_m}{J_m}\right) \tag{18}$$

$$h_3(t) = \frac{J_m}{K_t}\delta_4 \tag{19}$$

where $\omega_d(t)$ is now the time-varying frequency of the disturbance. The coefficients of $q(s)$ are constants as in (14). Fig. 5 shows the block diagram of the GS robust 2DOF speed regulator. Let $\hat{x}(t) = [x_1(t)\ x_2(t)\ x_3(t)]'$ and $\hat{u}(t) = [r(t)\ y(t) + n(t)]'$, the regulator can be implemented using the following observer canonical realization

$$\dot{\hat{x}}(t) = A_K(t)\hat{x}(t) + [B_{K1}(t) \quad B_{K2}(t)]\,\hat{u}(t)$$
$$u(t) = C_K(t)\hat{x}(t) + [D_{K1}(t) \quad D_{K2}(t)]\,\hat{u}(t)$$

where

$$\left[\begin{array}{c|cc} A_K(t) & B_{K1}(t) & B_{K2}(t) \\ \hline C_K(t) & D_{K1}(t) & D_{K2}(t) \end{array}\right] = \left[\begin{array}{ccc|cc} 0 & 1 & 0 & q_1 & -h_1(t) \\ -\omega_d^2(t) & 0 & 1 & q_2 - q_0\omega_d^2(t) & -h_2(t) + h_0(t)\omega_d^2(t) \\ 0 & 0 & 0 & q_3 & -h_3(t) \\ \hline 1 & 0 & 0 & q_0 & -h_0(t) \end{array}\right].$$

Since we need to deal with time-varying controller parameters, the transfer function argument is no longer valid and instead, the state space theory has to be invoked [17]. In the following, the stability of the time-varying closed loop system under the control by the proposed GS robust speed regulator is studied. The linearized AC PM motor system plant can be represented by the following state space equations:

$$\dot{x}_4(t) = -a_1 x_4(t) + b_1\,(u(t) + d(t))$$
$$y(t) = x_4(t)$$

where $a_1 = B_m/J_m$, $b_1 = K_t/J_m$, $x_4(t)$ is the state variable, $u(t)$ is the control input, $d(t)$ is the disturbance input and $y(t)$ is the control output. Let $\tilde{x}(t) = [x_1(t)\ x_2(t)\ x_3(t)\ x_4(t)]'$,

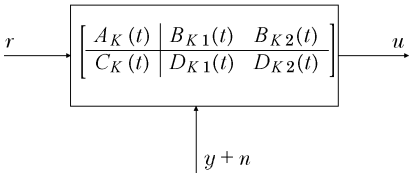

Fig. 5. The GS robust 2DOF speed regulator.

$\tilde{u}(t) = [r(t)\ d(t)\ n(t)]'$ and $\tilde{y}(t) = [u(t)\ y(t)]'$, the closed loop state space equations can be written as follows in reference to Fig. 4:

$$\dot{\tilde{x}}(t) = A(t)\tilde{x}(t) + B(t)\tilde{u}(t)$$
$$\tilde{y}(t) = C(t)\tilde{x}(t) + D(t)\tilde{u}(t)$$

where the system matrices are defined in (20).

The above system matrices can be transformed into an observer canonical form so as to facilitate the stability analysis by small gain theorem. A transformation matrix $P(t)$ is chosen accordingly to perform the task. Let $z(t) = [z_1(t)\ z_2(t)\ z_3(t)\ z_4(t)]'$ be the new state variables. With the following transformation

$$\tilde{x}(t) = P(t)z(t) = \begin{bmatrix} 0 & 0 & 1 & 0 \\ 0 & 1 & 0 & -\omega_d^2(t) \\ 1 & 0 & 0 & 0 \\ 0 & 0 & 0 & b_1 \end{bmatrix} z(t)$$

the closed loop system state space equations can be transformed into the following:

$$\dot{z}(t) = A_z(t)z(t) + B_z(t)\tilde{u}(t)$$
$$\tilde{y}(t) = C_z(t)z(t) + D_z(t)\tilde{u}(t)$$

where

$$\left[\begin{array}{c|c} A_z(t) & B_z(t) \\ \hline C_z(t) & D_z(t) \end{array}\right] = \left[\begin{array}{c|c} P^{-1}(t)A(t)P(t) - P^{-1}(t)\dot{P}(t) & P^{-1}(t)B(t) \\ \hline C(t)P(t) & D(t) \end{array}\right]$$

$$= \left[\begin{array}{ccc|c|cc} 0 & 0 & 0 & -\delta_4 & q_3 & 0 & -h_3(t) \\ 1 & 0 & 0 & -\delta_3 + \left(\omega_d^2(t)\right)' & q_2 & \omega_d^2(t) & -h_2(t) \\ 0 & 1 & 0 & -\delta_2 & q_1 & 0 & -h_1(t) \\ 0 & 0 & 1 & -\delta_1 & q_0 & 0 & -h_0(t) \\ \hline 0 & 0 & 1 & -b_1h_0(t) & q_0 & 0 & -h_0(t) \\ 0 & 0 & 0 & b_1 & 0 & 0 & 0 \end{array}\right]$$

see (20) at the bottom of the page.

The polynomial $\delta(s) = s^4 + \delta_1 s^3 + \delta_2 s^2 + \delta_3 s + \delta_4$ is the desired closed loop characteristic equation defined in Appendix A.

$$\left[\begin{array}{c|c} A(t) & B(t) \\ \hline C(t) & D(t) \end{array}\right] = \left[\begin{array}{ccc|c|cc} 0 & 1 & 0 & -h_1(t) & q_1 & 0 & -h_1(t) \\ -\omega_d^2(t) & 0 & 1 & -h_2(t) + h_0(t)\omega_d^2(t) & q_2 - q_0\omega_d^2(t) & 0 & -h_2(t) + h_0(t)\omega_d^2(t) \\ 0 & 0 & 0 & -h_3(t) & q_3 & 0 & -h_3(t) \\ b_1 & 0 & 0 & -a_1 - b_1h_0(t) & b_1q_0 & b_1 & -b_1h_0(t) \\ \hline 1 & 0 & 0 & -h_0(t) & q_0 & 0 & -h_0(t) \\ 0 & 0 & 0 & 1 & 0 & 0 & 0 \end{array}\right] \tag{20}$$

According to the small gain theorem [16], the associated autonomous system

$$\dot{z}(t) = A_z(t)z(t) = \left(\begin{bmatrix} 0 & 0 & 0 & -\delta_4 \\ 1 & 0 & 0 & -\delta_3 \\ 0 & 1 & 0 & -\delta_2 \\ 0 & 0 & 1 & -\delta_1 \end{bmatrix} + \begin{bmatrix} 0 \\ 1 \\ 0 \\ 0 \end{bmatrix} \left(\omega_d^2(t)\right)' \begin{bmatrix} 0 \\ 0 \\ 0 \\ 1 \end{bmatrix}' \right) z(t)$$

is internally uniformly exponentially stable if the following condition is satisfied:

$$\begin{aligned} &\left|\left(\omega_d^2(t)\right)'\right| \\ &< \left\| \begin{bmatrix} 0 \\ 0 \\ 0 \\ 1 \end{bmatrix}' \left(sI - \begin{bmatrix} 0 & 0 & 0 & -\delta_4 \\ 1 & 0 & 0 & -\delta_3 \\ 0 & 1 & 0 & -\delta_2 \\ 0 & 0 & 1 & -\delta_1 \end{bmatrix} \right)^{-1} \begin{bmatrix} 0 \\ 1 \\ 0 \\ 0 \end{bmatrix} \right\|_\infty^{-1} \\ &= \left\| \frac{s}{s^4 + \delta_1 s^3 + \delta_2 s^2 + \delta_3 s + \delta_4} \right\|_\infty^{-1} := r_S \end{aligned} \tag{21}$$

where r_S is defined as the stability radius. Therefore, as long as the input reference does not change too fast, the condition in (21) is satisfied, and the internal stability of the closed loop system is preserved. Since the matrices $B_z(t)$, $C_z(t)$ and $D_z(t)$ associated with the closed loop system are bounded, it follows from [17], the closed loop system is also bounded input bounded output (BIBO) stable if (21) is satisfied.

As $\omega_d(t) = (P/2)\omega_r(t)$, if the differentiation of the input speed reference $\omega_r(t)'$, or the acceleration profile, is available to the controller, then the stability radius can be further enlarged. By modifying the feedback gain $h_2(t)$ in (18) as:

$$h_2(t) = \frac{J_m}{K_t}\left[\delta_3 - \omega_d^2(t)\frac{B_m}{J_m} - \left(\omega_d^2(t)'\right)\right]. \tag{22}$$

Now the closed loop system matrices are given by

$$\left[\begin{array}{c|c} A_z(t) & B_z(t) \\ \hline C_z(t) & D_z(t) \end{array}\right] = \left[\begin{array}{cccc|ccc} 0 & 0 & 0 & -\delta_4 & q_3 & 0 & -h_3(t) \\ 1 & 0 & 0 & -\delta_3 & q_2 & \omega_d^2(t) & -h_2(t) \\ 0 & 1 & 0 & -\delta_2 & q_1 & 0 & -h_1(t) \\ 0 & 0 & 1 & -\delta_1 & q_0 & 1 & -h_0(t) \\ \hline 0 & 0 & 1 & -b_1 h_0(t) & q_0 & 0 & -h_0(t) \\ 0 & 0 & 0 & b_1 & 0 & 0 & 0 \end{array}\right].$$

As now $A_z(t)$ is a constant matrix and the other system matrices $B_z(t)$, $C_z(t)$ and $D_z(t)$ are bounded, the system is internally stable and BIBO stable.

In summary, the GS robust 2DOF regulators based on the IMP and the pole-zero placement algorithm can be implemented with an infinity stability radius provided that the differentiation of the input speed reference $\omega_r(t)'$ is available for the input of the GS robust 2DOF regulators. In this case, the new GS terms are given by (15)–(19) except that $h_2(t)$ is given by (22).

TABLE I
MOTOR PARAMETERS

J_m	0.144×10^{-4}kg·m^2
B_m	5.416×10^{-4}Nm/rad·s^{-1}
λ_m	0.0283Wb
L_d, L_q	11.5mH
R_s	6.8 Ω
P	8
$K_t = \frac{3}{2}\frac{P}{2}\lambda_m$	0.1698Nm/A
Encoder resolution	8000 counts/rev
Rated speed	1000rpm
Rated torque	0.48Nm
Rated voltage	200V (phase to phase)
Rated current	2.8A (phase)
Peak current	5.6A (phase)

TABLE II
DESIGN SPECIFICATIONS FOR A STEP INPUT

Overshoot	0%
Rise time	< 60ms

IV. SIMULATION RESULTS

Simulations are first performed to test the proposed control algorithm. A 50 W (rated mechanical power) AC PM motor is used in our simulations and experimental tests. The rated mechanical power is calculated using the formula $P_r = 2\pi N_r T_r$ where P_r is the rated mechanical power, N_r is the motor rated mechanical speed and T_r is the rated torque. The motor parameters are listed in Table I. The full motor model (1)–(4) is embedded in MATLAB/SIMULINK for the simulation purpose. Then we assume that a -0.08 A current offset is present at the current sensor of phase 1 and a 0.05 A current offset at the current sensor of phase 2. The above values are measured in the test platform. PI controllers are used in the current loop so that an approximated 1 kHz current loop bandwidth can be achieved. In comparison to the required rise time of the motion specification listed in Table II, the dynamics of the current loop is much faster than that of the speed loop; thus the assumption of the negligence of the current dynamics stated in Section II is justified.

The GS robust 2DOF speed regulator with the time-varying gain (15)–(19) is tested with three input profiles. With the addition of the acceleration profile input, the improved GS robust 2DOF speed regulator with the new time-varying gain (22) can be implemented so as to enlarge the stability radius.

The GS robust 2DOF speed regulator is first designed to satisfy the motion specifications listed in Table II. According to the design procedure listed in Section III, one of the possible solutions is to choose the four closed loop poles at -40, -50, -60 and -80, and the three closed loop zeros at -50, -60 and -80. Hence the overall system is a first order system with a single pole at -40, the slowest closed loop pole. With this selection, the rise time of the closed loop system is around $54\ \mathrm{ms} < 60\ \mathrm{ms}$ and the overshoot-free step response is automatically satisfied for a first-order low-pass system. The simulation results are shown in Fig. 7. Other choices of the pole and zero locations are possible but too fast closed loop poles may lead the signal saturation problem and the current loop dynamics may not be neglected if the bandwidth of the speed loop is close to that of

the current loops. The GS robust 2DOF speed regulator is implemented as in Fig. 5 with the following scheduled gains:

$$k_2(t) = 16\omega_r^2(t), \quad h_0(t) = 0.0163, \quad h_3(t) = 814.13$$
$$h_1(t) = 8.48 \times 10^{-5}\left(19400 - 16\omega_r^2(t)\right)$$
$$h_2(t) = 8.48 \times 10^{-5}\left(712\,000 - 601.78\omega_r^2(t)\right),$$

and the constant gains are

$$q_0 = 0.0032, \quad q_1 = 0.6445, \quad q_2 = 40.0283, \quad q_3 = 814.13.$$

The stability of this GS robust 2DOF speed regulator depends on the stability radius r_S and the differentiation of the input reference $|((P^2/4)\omega_r^2(t))'|$ in (21). Three input profiles with the conditions,

$$\left|\left(\frac{P^2}{4}\omega_r^2(t)\right)'\right| \ll r_S, \quad \left|\left(\frac{P^2}{4}\omega_r^2(t)\right)'\right| < r_S$$

and

$$\left|\left(\frac{P^2}{4}\omega_r^2(t)\right)'\right| > r_S,$$

are tested with the proposed GS robust 2DOF speed regulator.

The first input profile is shown in the upper section of Fig. 6. In the diagram, period 1 is used to test the GS robust 2DOF speed regulator in response to a step reference change from 0 to 50 rad/sec. Then in period 2 and period 4, the GS robust 2DOF speed regulator is tested with a ramp input. Finally, period 3, 5, and 6 are used for the high (rated speed), low and zero constant speed tests. The term $|((P^2/4)\omega_r^2(t))'|$ of the first profile is shown in Fig. 6 and it is found that the maximum value of $|((P^2/4)\omega_r^2(t))'| = 2.88 \times 10^5$ is approximately equal to half of the stability radius $r_S = 5.57 \times 10^5$. In order to demonstrate the effectiveness of the use of the IMP, another robust 2DOF regulator is designed without including the sinusoidal disturbance modes. This can be done by simply assigning $k(s) = s$ in (9) and the dominant closed loop pole of this robust 2DOF regulator is also placed at -40, the same one of the GS robust 2DOF speed regulator. The upper section of Fig. 7 shows the output speed response when the robust 2DOF regulator excluding the sinusoidal disturbance modes is used; the output speed is contaminated with ripples caused by the DC current offset torque ripples. On the other hand, with the help of the sinusoidal modes inside the speed regulator, the output speed response of the GS robust 2DOF speed regulator shown in the lower section of Fig. 7, achieves a desirable tracking response without any velocity ripple contamination. In addition, the motion specifications listed in Table II are also satisfied when the GS robust 2DOF speed regulator is used.

The sinusoidal disturbance torque is actually compensated by the signal generated from the sinusoidal modes that we assigned in the GS robust 2DOF speed regulator. The lower section of Fig. 8 shows the torque command at the output of the GS robust 2DOF speed regulator. The sinusoidal signal generated at the torque command can compensate the time-varying sinusoidal disturbance so that no velocity ripple can be found at the motor output speed. On the other hand, the torque command of the robust 2DOF regulator excluding the sinusoidal modes is shown in the upper section of Fig. 8; the sinusoidal signal present at this

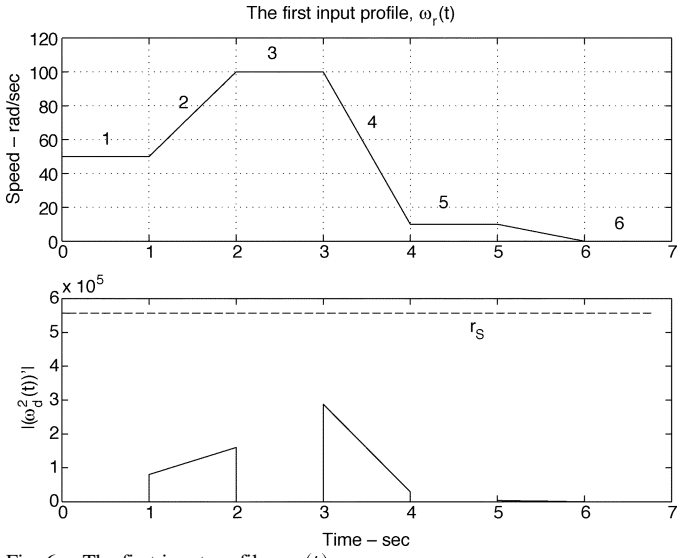

Fig. 6. The first input profile, $\omega_r(t)$.

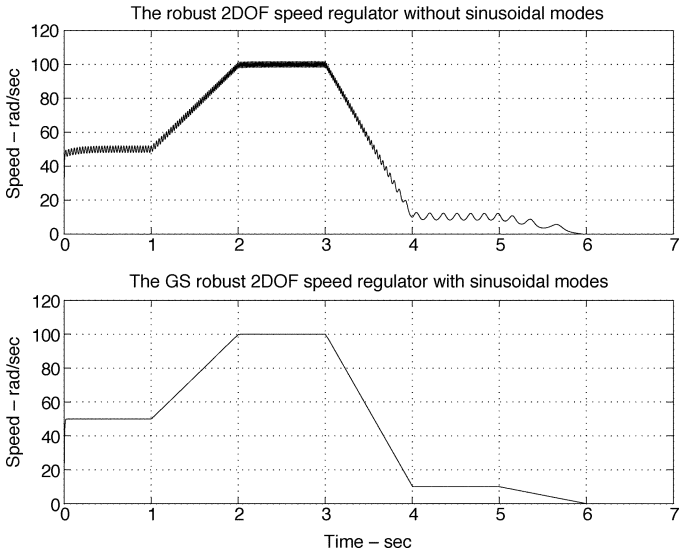

Fig. 7. The speed output responses.

torque command is derived from the contaminated speed output and cannot compensate for the time-varying sinusoidal disturbance. The frequency spectrums of the error speed responses are shown in Fig. 9. This spectrum plot is performed by subtracting the frequency spectrum of the output speed response from the one of the time-varying step reference input. When the robust 2DOF regulator excluding the disturbance modes is used, the error speed frequency spectrum has three large component frequencies at 40 rad/sec, 200 rad/sec and 400 rad/sec which correspond to the three constant speed tracking periods at 10 rad/sec, 50 rad/sec and 100 rad/sec. The error speed spectrum of the motor control system using the GS robust 2DOF speed regulator has a low value at all frequency. All the above results demonstrated that the use of the IMP to eliminate the torque and velocity ripples caused by DC current offsets is necessary and effective.

The second profile used in the simulation test is shown in Fig. 10. The acceleration rate of this profile is larger so that the maximum value of $|((P^2/4)\omega_r^2(t))'|$ is closer to the stability radius r_S. The upper section of Fig. 11 shows the

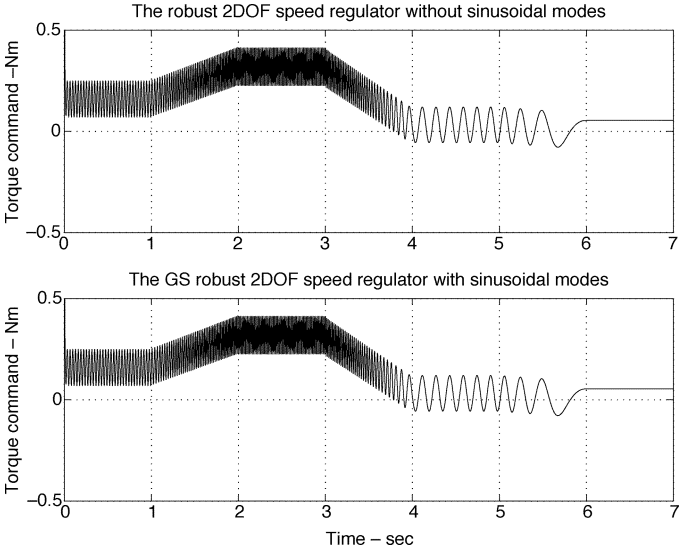

Fig. 8. The torque command.

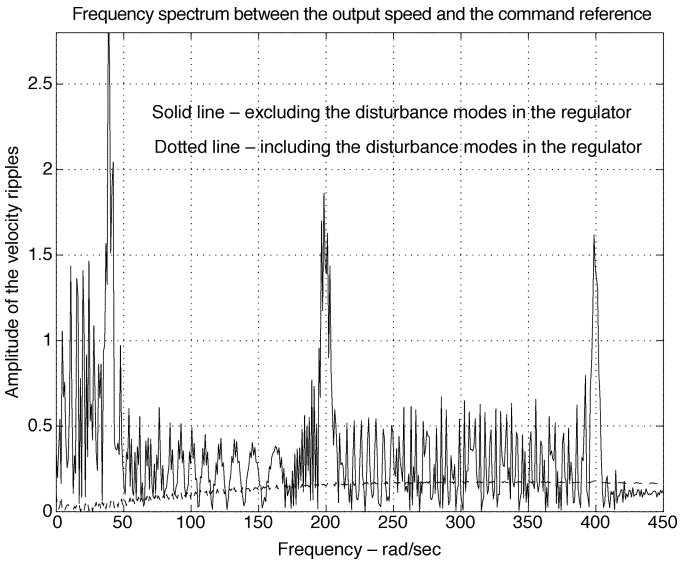

Fig. 9. The frequency spectrum of the speed error.

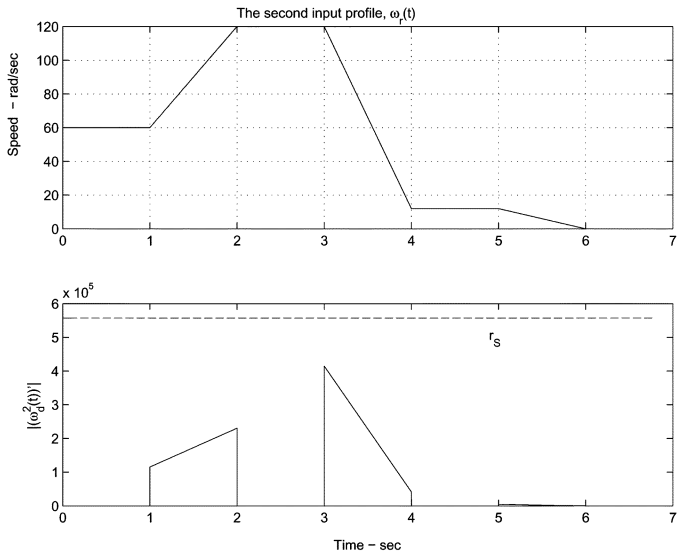

Fig. 10. The second input profile, $\omega_r(t)$.

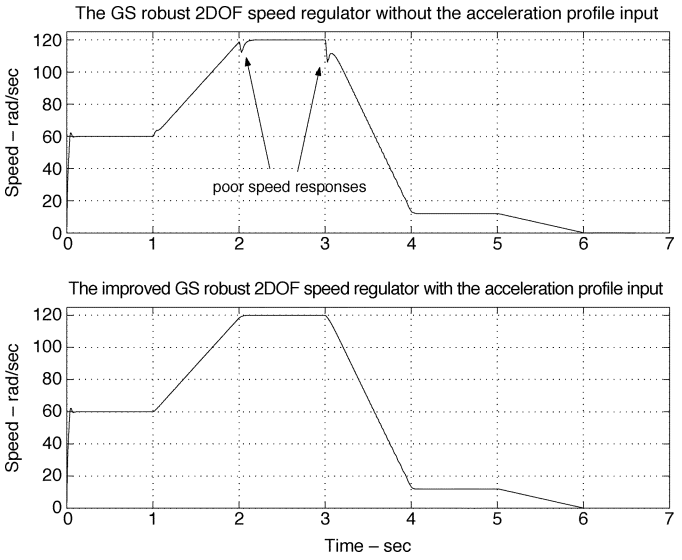

Fig. 11. The output speed responses.

output speed response; the poor speed responses can be found at the turning corners at $t = 2s$ and $t = 3s$ when the value of $|((P^2/4)\omega_r^2(t))'|$ approaches the stability radius. As discussed in Section III-B, the stability radius can be enlarged to infinity if the term $((P^2/4)\omega_r^2(t))'$, or the acceleration profile, is available for the use by the GS controller. Then the improved GS robust 2DOF speed regulator is implemented with the following new gain defined in (22):

$$h_2(t) = 8.48 \times 10^{-5}\left[712\,000 - 571.78\omega_r^2(t) - 16\left(\omega_r^2(t)\right)'\right].$$

The same input profile is tested with the improved GS robust 2DOF speed regulator and the output speed response is shown in the lower section of Fig. 11. The desirable tracking responses can be retrieved at the two turning corners. Therefore, the improved GS robust 2DOF speed regulator with the acceleration profile input is concluded to be the most effective controller in the elimination of the torque and velocity ripples caused by DC current offsets.

To further test the proposed GS robust 2DOF speed regulator, the third profile with the maximum value of $|((P^2/(4)\omega_r^2(t))'| > r_S$ is shown in the upper section of Fig. 12. Without the acceleration profile input, the speed response is shown in the upper section of Fig. 13; the output speed response is not good in general and at $t = 3s$, as the value of $|((P^2/4)\omega_r^2(t))'| > r_S$, the output speed becomes unstable and oscillatory. However, if the improved GS robust 2DOF speed regulator is implemented with the acceleration profile input, a comparatively good speed response is obtained and shown in the lower section of Fig. 13, and the stability of the whole system remains. Smooth transitions can still be maintained during the high speed turning corners at $t = 2s$ and $t = 3s$. This simulation result shows the stability radius of the overall system can be enlarged with the availability of the acceleration input profile.

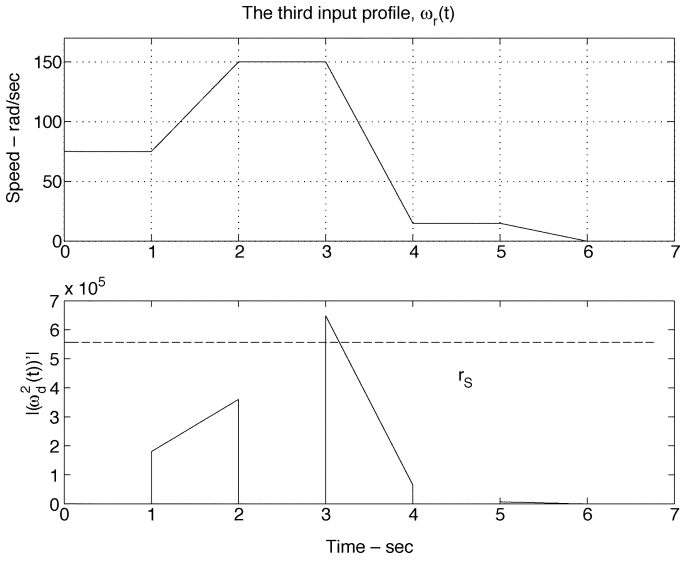

Fig. 12. The third input profile, $\omega_r(t)$.

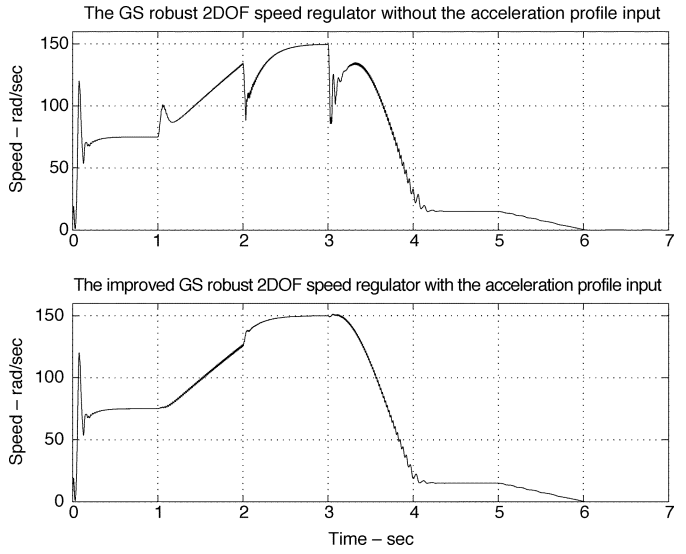

Fig. 13. The output speed responses.

V. Experimental Results

Experiments are performed to further verify the effectiveness of our proposed GS robust 2DOF speed regulators. Fig. 1 shows the basic setup of our experiment. A dSPACE DS1102 DSP controller board is used as our motion controller. In connection with a MATLAB real-time workshop and SIMULINK, a fast prototyping working environment is achieved and, hence, code development time can be saved. The DSP controller implements all control algorithms with a sampling frequency 4 kHz. In every control cycle the controller reads the motor encoder, performs the control algorithm calculation, and then outputs two current reference commands i_a and i_b to the current tracking amplifier. The current tracking amplifier employed in the experiment can deliver a rated current of 3 A and a peak current of 6 A. The rated voltage of this motor amplifier is 200 V. The parameters of the AC PM motor used in the test bed is listed in Table I. The current driving capability of the motor amplifier is matched with the AC PM motor because the rated current and the peak current

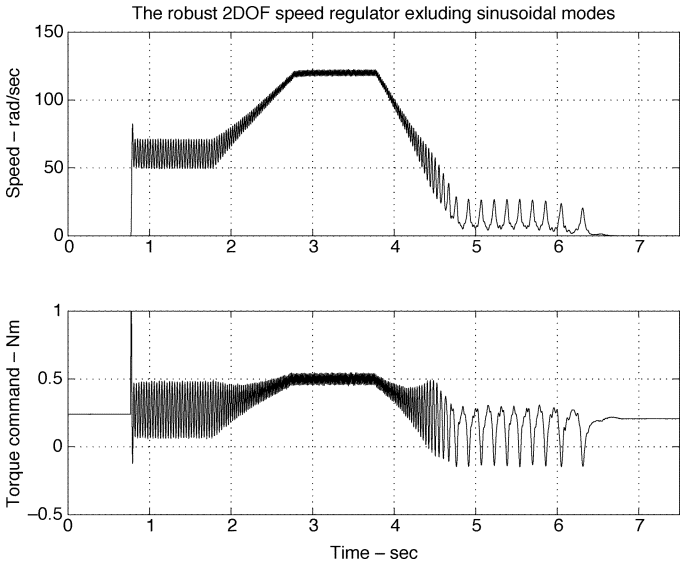

Fig. 14. The speed response of the robust 2DOF speed regulator without the sinusoidal modes.

of the motor amplifier are barely above the ones of the AC PM motor.

In the practical experiment, the improved GS robust 2DOF speed regulator with the acceleration profile input is implemented as in Fig. 5. The constant and time-varying scheduled gains are listed as below:

$$\begin{aligned} q_0 &= 0.0032,\ q_1 = 0.6445,\ q_2 = 40.0283,\ q_3 = 814.13 \\ k_2(t) &= 16\omega_r^2(t),\ h_0(t) = 0.0163,\ h_3(t) = 814.13 \\ h_1(t) &= 8.48 \times 10^{-5}\left(19400 - 16\omega_r^2(t)\right) \\ h_2(t) &= 8.48 \times 10^{-5}\left[712\,000 - 571.78\omega_r^2(t) - 16\left(\omega_r^2(t)\right)'\right]. \end{aligned}$$

After setting up the whole system, the current offset values of phase 1 and 2 at that particular time are measured and equal to 0.1 A and 0.09 A respectively. These values are different from the ones used in Section IV because the two measurement are made at different time and different operating temperature of the motor driver. This also indicated that the offline compensation cannot perform satisfactorily as the DC current offset values drift with time and temperature. It should be emphasized that the measured current offset values are never used in the speed regulator design and the implementation so as to eliminate the torque ripples.

The second profile described in the previous section is employed as the input in this practical experiment. In addition, the robust 2DOF speed regulator without the sinusoidal modes, stated in the previous section, is used to compare with the improved GS robust 2DOF speed regulator with the sinusoidal modes. The dominant closed loop poles of the two regulators are the same. The speed response of the motor system controlled using the robust 2DOF speed regulator without the sinusoidal modes is shown in Fig. 14 and the speed output is contaminated with ripples. This concludes that a single integrator inside the regulator cannot generate a proper signal to eliminate the torque ripples. Fig. 15 depicts the speed response when the improved GS robust 2DOF speed regulator is used;

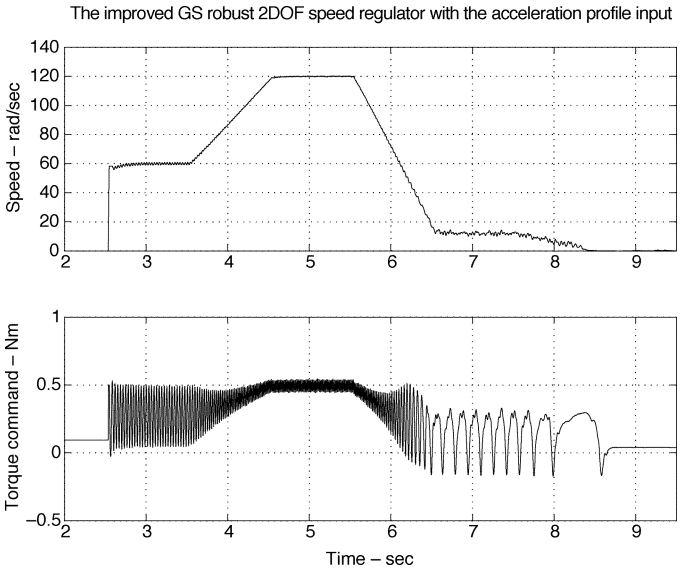

Fig. 15. The speed response of the improved GS robust 2DOF speed regulator with the sinusoidal modes.

the output speed does not contain any ripple and achieves a desirable tracking response. The motion specifications listed in Table II are also satisfied. The time-varying sinusoidal modes inside the regulator can generate an equal but opposite signal to eliminate the torque and velocity ripples cause by the DC current offsets.

The frequency spectrums of the speed error are shown in Fig. 16. There are three large frequency components at 48 rad/sec, 240 rad/sec and 480 rad/sec if the robust 2DOF speed regulator without the sinusoidal modes is used. These three frequency components are corresponding to the three constant speed tracking periods at 12 rad/sec, 60 rad/sec and 120 rad/sec respectively. These frequency components are reduced almost to zero if the improved GS robust 2DOF speed regulator with the sinusoidal modes is employed. In addition, the error speed frequency spectrum of the improved GS robust 2DOF speed regulator has a low value at all frequency, this justifies the assumption made in Section I that the AC PM motor used in the control system has negligible cogging, reluctance and mutual torque. Finally, Fig. 17 shows the input phase 1 current command (Channel 3) and the actual phase 1 output current value (Channel 2) when the speed reference input is the second profile stated in the previous section; they track closely and this validates that the current loop bandwidth is adequate in this application and the assumption of the negligence of the current dynamics stated in Section II is further justified.

The experimental results shown in this section match the simulation results. This demonstrated that the improved GS robust 2DOF speed regulator based on the IMP is an effective solution to eliminate the torque ripples in an AC PM motor control system.

VI. Conclusions

In this paper the use of IMP to eliminate the torque and velocity ripples caused by DC current offsets in AC PM control systems is demonstrated to be an novel and effective solution. The model of the torque ripples caused by DC current offsets is developed. Then a GS robust 2DOF speed regulator based on the IMP is designed to eliminate the torque and velocity ripples for a time-varying speed step reference. The stability of this speed regulator depends on the closed loop system poles and the availability of the acceleration input profile. Another improved GS robust 2DOF speed regulator with the addition of the acceleration profile input, is constructed so as to maintain the stability of the closed loop system all the time. Simulation and experimental results reveal that the improved GS robust 2DOF speed regulator can eliminate the torque and velocity ripples successfully in an AC PM motor control system. The proposed GS robust 2DOF speed regulators can include the sinusoidal modes with different frequencies so as to compensate other torque ripples such as the mutual, reluctance or cogging torque.

The improved GS robust 2DOF speed regulator design to eliminate the torque and velocity ripples caused by DC current offsets is dedicated to the automation machinery manufacturing. With this speed regulator, common and low-cost current sensors and digital-to-analog converters can still be used in AC PM motor control systems; operators and service engineers do not need to trim the offset values periodically. Thus the total cost of an automation machine can be reduced and the output system performance can be enhanced.

The regulator design algorithm discussed in this paper is not limited to the torque ripples of AC PM motor control systems due to DC offsets, but can also be generalized to the rejection of any other torque ripples and sinusoidal external load torque with known frequencies.

Appendix

A. Design of Robust 2DOF Regulators

In this appendix, we present a design procedure for robust 2DOF regulators shown in Fig. 3. Robust 2DOF regulators were discussed in [11] and [12], in which the disturbance and reference are assumed to have the same modes. In the following we assume that they may have different modes. Here the plant $G(s)$ is assumed to be a general single input single output (SISO) system while the reference input, $r(t)$, and the disturbance input, $d(t)$, are assumed to have possibly different modes. The design is based on a pole-zero placement technique.

Let $G(s)$ be a SISO plant described by a strictly proper transfer function $G(s) = b(s)/a(s)$, where

$$a(s) = s^{n_a} + a_1 s^{n_a-1} + \cdots + a_{n_a} \tag{23}$$

$$b(s) = b_1 s^{n_a-1} + b_2 s^{n_a-2} + \cdots + b_{n_a} \tag{24}$$

and it is assumed that $a(s)$ and $b(s)$ are coprime. The general 2DOF controller shown in Fig. 3 can be written as:

$$[K_1(s) \quad -K_2(s)] = \frac{1}{k(s)}[q(s) \quad -h(s)] \tag{25}$$

where

$$k(s) = s^{n_k} + k_1 s^{n_k-1} + \cdots + k_{n_k} \tag{26}$$

$$q(s) = q_0 s^{n_k} + q_1 s^{n_k-1} + \cdots + q_{n_k} \tag{27}$$

$$h(s) = h_0 s^{n_k} + h_1 s^{n_k-1} + \cdots + h_{n_k}. \tag{28}$$

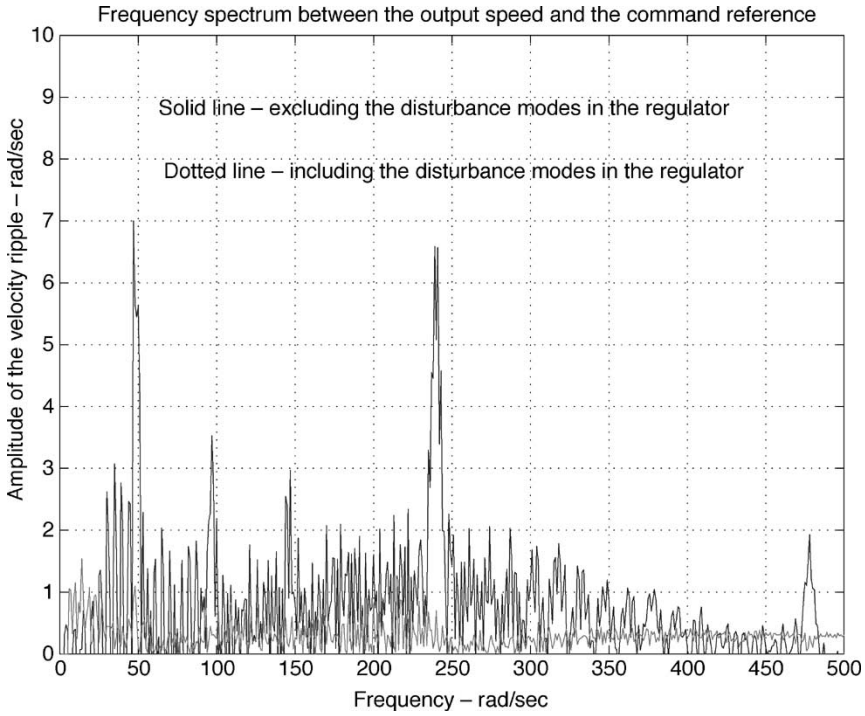

Fig. 16. The speed response of the speed error.

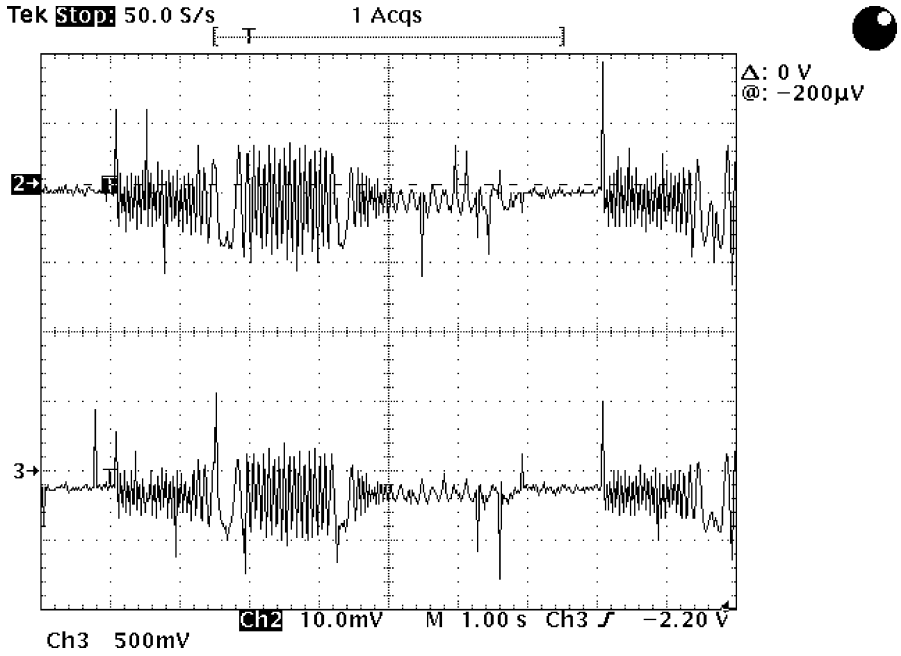

Fig. 17. The current response. Ch 2—Actual phase 1 current (1 A/10 mV). Ch 3—phase 1 current command.

The 2DOF control structure then becomes as shown in Fig. 4. The transfer function from the input reference to the output is given by

$$\frac{Y(s)}{R(s)} = \frac{b(s)q(s)}{a(s)k(s)+b(s)h(s)} := \frac{b(s)q(s)}{\delta(s)}$$

and the transfer function from the disturbance input to the output is given by

$$\frac{Y(s)}{D(s)} = \frac{b(s)k(s)}{\delta(s)}.$$

Let the unstable modes of $r(t)$ be the roots of monic polynomial $m_r(s)$ and those of $d(t)$ be the roots of $m_d(s)$. Let the least common multiple of $m_r(s)$ and $m_d(s)$ be $m(s)$. It is well-known that the robust regulator problem is solvable, i.e., it is possible to design a controller so that the disturbance rejection and reference tracking are achieved, if and only if $m(s)$ and $b(s)$ are coprime. Now assume that this condition is satisfied. Physically, according to the IMP [12], both the disturbance rejection and reference tracking can be achieved robustly if the unstable modes of the reference and disturbance are included in

the controller. Mathematically, a solution to the robust regulator problem [12] must satisfy

$$k(s) = g(s)m(s) \tag{29}$$

and

$$h(s) - q(s) = f(s)m_r(s) \tag{30}$$

where $g(s)$ and $f(s)$ are polynomials. Therefore, the design of the robust 2DOF regulator amounts to the determination of polynomials $f(s)$, $g(s)$ and $h(s)$. A simple yet systematic way to design $g(s)$ and $h(s)$ is to use the pole placement algorithm. Denote

$$g(s) = s^{n_g} + g_1 s^{n_g - 1} + \ldots + g_{n_g}. \tag{31}$$

The closed loop characteristic polynomial is

$$k(s)a(s) + h(s)b(s) = g(s)m(s)a(s) + h(s)b(s) := \delta(s). \tag{32}$$

Note that $\delta(s)$ is a monic polynomial of degree $n_g + n_m + n_a$. The purpose of pole placement is to design $g(s)$ and $h(s)$ so that the roots of $\delta(s)$ are arbitrarily assigned. Since $m(s)a(s)$ and $b(s)$ are coprime, it can easily be shown that the pole placement is possible if and only if

$$n_g \geq n_a - 1. \tag{33}$$

If this condition is satisfied, the coefficients of $g(s)$ and $h(s)$ can be obtained by equating the coefficients of both sides of (32). To eliminate the controller complexity we can choose $n_g = n_a - 1$. After $g(s)$ and $h(s)$ are designed the closed loop transfer function from $r(t)$ to $y(t)$ becomes

$$\frac{Y(s)}{R(s)} = \frac{q(s)b(s)}{\delta(s)} = \frac{[h(s) - f(s)m_r(s)]\,b(s)}{\delta(s)}. \tag{34}$$

We wish to design $f(s)$ so that the undetermined n_k zeros of this transfer function, i.e., the roots of $h(s) - f(s)m_r(s)$, can be assigned in a desirable way. In general, $f(s)$ does not have enough degree of freedom to assign arbitrarily the roots of $h(s) - f(s)m_r(s)$. However, if the reference is a step function, then $m_r(s) = s$ and the $n_k - 1$ coefficients of $f(s)$ can be used to assign all, but one coefficients of $h(s) - f(s)m_r(s)$ and, hence, all roots of $h(s) - f(s)m_r(s)$. Therefore, in the case when the reference is a step function, n_k zeros of $Y(s)/R(s)$ can be arbitrarily assigned.

REFERENCES

[1] D. Chen and B. Paden, "Adaptive linearization of hybrid step motors: stability analysis," *IEEE Trans. Automat. Contr.*, vol. 38, pp. 874–887, June 1993.

[2] Y. Liu and D. Chen, "Adaptive rejection of velocity-ripple from position transducer in a motion control system," in *Proc. 33rd IEEE Conf. Decision and Control*, 1994, pp. 690–695.

[3] V. Petrovic, R. Ortega, A. M. Stankovic, and G. Tadmor, "Design and implementation of an adaptive controller for torque ripple minimization in PM synchronous motors," *IEEE Trans. Power Electron.*, vol. 15, pp. 871–880, Sept. 2000.

[4] G. Ferretti, G. Magnani, and P. Rocco, "Modeling, identification, and compensation of pulsating torque in permanent magnet AC motors," *IEEE Trans. Ind. Electron.*, vol. 45, pp. 912–920, Apr. 1998.

[5] T. M. Jahns and W. L. Soong, "Pulsating torque minimization techniques for permanent magnet AC motor drive—a review," *IEEE Trans. Ind. Electron.*, vol. 43, pp. 321–330, Apr. 1996.

[6] C. Studer, A. Keyhani, T. Sebastain, and S. K. Murthy, "Study of cogging torque in permanent magnet machines," in *Proc. 32nd IEEE IAS Annual Meeting*, vol. 1, 1997, pp. 42–49.

[7] T. Li and G. Slemon, "Reduction of cogging torque in permanent magnet motors," *IEEE Trans. Magn.*, vol. 24, pp. 2901–2903, June 1988.

[8] S. O. Bogosyan and M. Gokasan, "Adaptive torque ripple minimization of permanent magnet synchronous motors for high-performance direct-drive applications," in *Proc. 30th IEEE IAS Annual Meeting*, vol. 1, 1995, pp. 231–237.

[9] S. K. Chung, H. S. Kim, C. G. Kim, and M. J. Youn, "A new instantaneous torque control of PM synchronous motor control," *IEEE Trans. Power Electron.*, vol. 13, pp. 388–400, Mar. 1998.

[10] D. W. Novotny and T. A. Lipo, *Vector Control and Dynamics of AC Drives*. New York: Oxford, 1998.

[11] M. Vidyasagar, *Control System Synthesis*. Cambridge, MA: MIT Press, 1985.

[12] W. A. Wolovich, *Automatic Control Systems*. Fort Worth, TX: Sauders College Publishing, 1994.

[13] P. Vas, *Vector Control of AC Machines*. New York: Oxford, 1990.

[14] FLI. Boldea and S. A. Nasar, *Electric Drives*. Boca Raton: CRC, 1999.

[15] E. J. Davison and A. Goldberg, "Robust control of a general servomechanism problem: the servo compensator," *Automatica*, vol. 11, pp. 461–471, 1975.

[16] C. A. Desoer and M. Vidyasagar, *Feedback Systems: Input-Output Properties*. New York: Academic, 1975.

[17] W. J. Rugh, *Linear System Theory*. Englewood Cliffs, NJ: Prentice-Hall, 1996.

Wai-Chuen Gan (S'94-M'02) received the B.Eng degree, with first class honors and academic achievement awards, in electronic engineering, and the M.Phil. and Ph.D. degrees in electrical and electronic engineering from The Hong Kong University of Science and Technology, Hong Kong, in 1995, 1997, and 2001, respectively.

From 1997 to 1999, he was with ASM Assembly Automation Ltd., as a Motion Control Application Engineer, and 2002, he again joined ASM where he is responsible for the development of the digital motor drivers. His current research interests include robust control of AC machines, power electronics, design and control of linear switched reluctance motors, and control of stepping motors.

Li Qiu (S'85-M'90-SM'98) received the B.Eng degree in electrical engineering from Hunan University, Changsha, Hunan, China, in 1981, and the M.A.Sc. and Ph.D. degrees in electrical engineering from the University of Toronto, Toronto, ON, Canada, in 1987 and 1990, respectively.

Since 1993, he has been with the Department of Electrical and Electronic Engineering, Hong Kong University of Science and Technology, Clear Water Bay, Kowloon, Hong Kong SAR, China, where he is currently an Associate Professor. He has also held research and teaching positions in the University of Toronto, Canadian Space Agency, University of Waterloo, University of Minnesota, Zhejiang University, and Australia Defence Force Academy. His current research interests include systems control theory, signal processing, and control of electrical machines.

He served as an Associate Editor of the IEEE TRANSACTIONS ON AUTOMATIC CONTROL and an Associate Editor of *Automatica*.